Journal of Materials Chemistry A

Accepted Manuscript

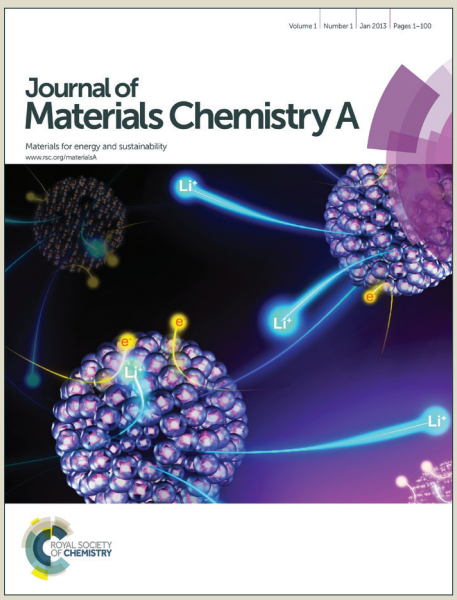

ROYAL SOCIETY OF CHEMISTRY

www.rsc.org/materialsA

Contents page

Sandwich-type N-doped graphene based carbon materials with wrinkled sheet-like morphology were prepared and demonstrated remarkable performances as supercapacitor electrodes.

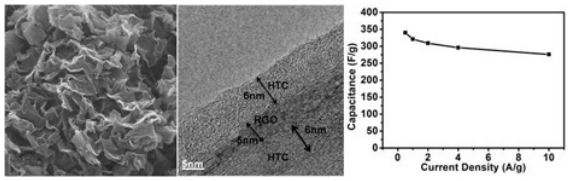

Journal Name

RSCPublishing

ARTICLE

Synthesis of hierarchical porous N-doped sandwich-type carbon composites as high-performance supercapacitor electrodes

Cite this: DOI: 10.1039/x0xx00000x

Received 00th January 2012,
Accepted 00th January 2012

DOI: 10.1039/x0xx00000x

www.rsc.org/

Huaxing Luo, Zhenyu Liu, Lumeng Chao, Xiaochao Wu, Xiaodong Lei, Zheng Chang*, Xiaoming Sun*

Sandwich-type graphene based N-doped carbon materials (RGO@HTC) were prepared by in situ carbonization of glucose molecules on the surface of graphene oxide sheets in the presence of ethylenediamine (EDA), followed by KOH activation to further enhance the porosity. The results revealed that hydrothermal carbon layers uniformly coated both sides of graphene sheets, achieving sandwich-type composites with a hierarchical porous structure. The introduction of EDA with two amino terminals not only ensured the nitrogen doping into carbon composites, but also induced the hydrothermal carbonization of glucose to take place on the surface of GO as a binder. The influences of reactant ratio, activation reagent amount, activation temperature on morphology, structure and electrochemical performance were systematically studied. Under the optimized conditions, the carbon composites demonstrated remarkable electrochemical performances as supercapacitor electrodes with an outstanding specific capacitance of 340 F g^{-1} at a current density of 0.5 A g^{-1}, and retained 203 F g^{-1} at a high current density of 50 A g^{-1} in 6 mol L^{-1} KOH. Moreover, the cycling stability was quite well without any decay after 2000 cycles. The outstanding supercapacitor performance was considered to be related to the large surface area, appropriate hierarchical pore structure, N-doping and good electrical conductivity of the RGO@HTC. The electrochemical performance coupled with a facile and low-cost preparation procedure ensured the resulting RGO@HTC as promising electrode materials for supercapacitor applications.

1 Introduction

Supercapacitors have attracted intense interest as ideal energy storage devices due to their high power capacity, long cycle life and cleanness, especially in high power delivery or uptake needed applications.[1-5] Carbon materials are considered to be the most attractive candidates as supercapacitor electrodes owing to their high electrical conductivity, large surface area and low cost.[6] Various carbon materials including porous activated carbon,[7,8] carbon nanotube,[9-11] carbon foam,[12] porous carbon micro- /nanosphere,[13-15] ultramicroporous carbon nanoparticle[16] and graphene[17-20] have been demonstrated for high-performance supercapacitors. Recently, carbon-based materials derived from plant biomass show great advantages when considering the potential scale of supercapacitor applications[21,22]. Biomass is a cost-effective carbon precursor because it is available in high quality and abundance, and is an environmental friendly renewable resource. Moreover, hydrothermal carbonization of biomass is a facile route to synthesis these carbon materials with controlled structures and sizes.[22,23] These hydrothermal carbon materials (HTCs) could inherit hydrophilicity/lipophilicity of the biomass precursor, leading to the enhanced wettability and rapid electrolytic ion transport. With this in mind, HTCs have been considered as promising candidates of electrode materials for supercapacitors. However, they always suffer from the poor conductivity, which seriously limits their supercapacitor performances at large current densities. Combining HTCs and conductive substrates should effectively solve this problem.

Graphene, a two-dimensional all-sp^2-hybridized carbon, has received immense interest due to its extraordinary conductivity, high surface area, good elasticity and stiffness.[17,19,24-26] Graphene sheets and chemically modified graphene-based materials are widely regarded as potential supercapacitor electrode materials. But in fact, the practical applications of graphene electrodes in a large scale remain being an issue. On

the one hand, when prepared in the form of reduced graphene oxide (rGO) via the established solution processes, typical specific capacitances of graphene materials exhibit only 100-150 F g^{-1} in organic electrolytes [24,27,28] and 150-230 F g^{-1} in inorganic electrolytes,[18,29,30] which is far from the theoretical capacitance as high as 550 F g^{-1}.[24] The lower capacitances are mainly related to irreversible restacking of these individual rGO sheets during the reduction and drying processes,[27-29] which makes substantial surfaces of rGO unavailable for charge storage. On the other hand, these synthesis conditions are quite harsh during the chemical reduction of graphene oxide (GO).[31-33] And this method is of low productivity and the reductive reagents are generally hazardous or toxic.[34] Moreover, for having high supercapacitor performances, some special post-treatment processes may be needed, like freeze drying or plasma treating,[35] which also hinder their practical applications. Thus, the scale-up production of graphene-based materials with considerable supercapacitor characteristics also remains challenging.

Recently, investigators began to synthesis some carbon composites combining GO with biomass as supercapacitor electrodes, which would unite their respective advantages together. J. Huang *et al.*[36] demonstrated that the addition of a small amount of GO could greatly improve the electrochemical properties of biomass derived carbon, whereas the specific capacitance of 140 F g^{-1} (at 1 A g^{-1}) was not so attractive. J. Qiu *et al.*[37] reported a nitrogen-rich graphene incorporated HTCs composite with a high specific capacitance of 300 F g^{-1} (at 0.1 A g^{-1}). But using glucosamine molecules as carbon precursor and nitrogen source is not really cost-effective for the preparation of carbon materials. Therefore, it is expected that cheap graphene-based carbon materials with high supercapacitor performances could be produced in the future.

In this work, we prepared N-doped hydrothermal carbon coated graphene composites (RGO@HTC) by carbonization of biomass glucose on the surface of GO under the help of ethylenediamine (EDA). In this one-step synthesis process, GO was used as conductive substrate and glucose acted as building block and reductive reagent. EDA not only doped the composites with nitrogen, but also induced hydrothermal carbonization of glucose to take place on the surface of GO sheets due to the electrostatic attractions between its amino terminal and negatively charged GO or glucose, leading to the formation of HTCs coated rGO. The obtained composites were further activated by KOH to enhance the porosity. Depending on the good electrical conductivity of rGO substrate and the rich porosity of hydrothermal carbon surface, the RGO@HTC composites exhibited remarkable supercapacitor performances with a high specific capacitance, rate capacity and cycle stability. Moreover, the final composites had significantly increased masses, which could effectively offset the shortcoming of low productivity of rGO. The excellent supercapacitor performance and low-cost preparation of RGO@HTC composites would potentially pave the pathway for practical supercapacitor applications.

2 Experimental

All chemicals were of analytical grade and purchased from Beijing Chemical Reagents Company. All the reagents were used without any purification and deionized water was used in all experiments.

2.1 Synthesis of RGO@HTC

Firstly, graphite oxide (GO) was prepared from graphite by a modified Hummer's method. The prepared solid GO (1.25 g) was dispersed in water (250 mL) under ultrasonication to prepare a GO aqueous dispersion (5 mg mL^{-1}). Then, 8 ml GO aqueous dispersion was mixed with a certain volume of ethylenediamine (EDA) from 0.5, 1 to 2 mL, and stirred for 1 h. Afterwards, a certain mass of glucose was added into the mixture and some water was supplied to ensure the total solution volume up to 40 mL. The weight ratios of glucose to GO were respectively adjusted from 25:1, 50:1, 100:1 to 200:1. After stirring for 30 min, the resulting solution was sealed into a 40 ml Teflon-lined stainless steel autoclave, followed by hydrothermal treatment at 180°C for 10 h. After cooling naturally, the products were washed 3 times with water and dried at 80 °C over night in vacuum. Finally, the hydrothermal carbonized samples were mixed with KOH at different weight ratios (4:1, 3:1, 2:1, 1:1 or 1:2), and then heated at different temperature (500, 550, 600, 650 or 700°C) for 2 h under inert atmosphere (N_2). The final samples were collected after washing with diluted hydrochloric acid and water until neutral pH and drying at 80 °C over night, denoted as RGO@HTC.

For comparison, two control samples were prepared via the same hydrothermal treatment and KOH activation processes without GO or EDA, denoted as Glu/EDA and Glu/GO, respectively.

2.2 Characterization

The element contents of carbon, oxygen, and nitrogen in the samples were determined using a Vario EL Elemental instrument. Nitrogen adsorption and desorption isotherms were measured at 77 K with a Quadrachrome Adsorption Instrument. Prior to the measurements, the samples were degassed at 150 ºC in vacuum for 20 h. The Brunaer-Emmett-Teller (BET) and Barrett-Joyner-Halenda (BJH) methods were used for the specific surface area determination and pore size distribution calculation, respectively. The size and morphology of the samples were observed from scanning electron microscope (SEM, Zeiss Supra 55) and transmission electron microscopy (TEM, FEI Technai G2 F20 microscope). High-resolution transmission electron microscopy (HRTEM) experiments were recorded on a JEM 2100. The X-ray diffraction (XRD) data were collected with a Shimadzu XRD-6000 diffractometer with Cu Kα radiation (λ=1.5418 Å). Raman spectra were recorded

on the Lab RAM ARAMIS Raman system with a 532 nm argon ion laser as excitation. XPS measurements were performed using a Thermo Electron ESCALAB 250 instrument with Al Kα radiation. Zeta potential measurements were carried out in a ZS90 Malvern Zetasizer instrument.

2.3 Electrochemical measurements

Cyclic voltammetry (CV), galvanostatic charge/discharge (GCD) and electrochemical impedance spectroscopy (EIS) measurements were carried out in a one-compartment cell in 6 mol L^{-1} KOH aqueous solution using a three-electrode configuration on a CHI 660D (Shanghai Chenhua) electrochemical workstation. In a typical procedure, the electrode was prepared by mixing active materials (80 wt%), conductive graphite (15 wt%), and polytetrafluoroethylene (PTFE) binder (5 wt%) well in appropriate volume of ethanol. Platinum foil and Hg/HgO (0.052 V vs. a normal hydrogen electrode, NHE) were used as counter electrode and reference electrode, respectively. The specific capacitances (C) in this paper were calculated from GCD curves according to the equation: $C = I\,t\,/\,m\,\Delta V$, where I was the charge/discharge current density, t was the discharge time, Δ V was the voltage difference, and m was the mass of the loaded active materials.

3 Results and discussion

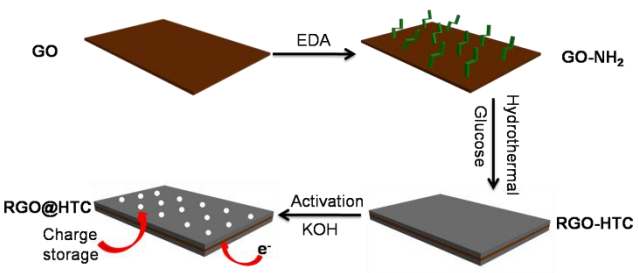

Fig. 1 Schematic of the proposed formation mechanism of RGO@HTC.

The strategy to prepare graphene based carbon composites (RGO@HTC) is schematically shown in Fig. 1. Firstly, GO sheets with heavily oxygenated surfaces and negative charges were obtained by a modified Hummer's method.[38] Afterwards, ethylenediamine (EDA) with two amino terminals was chosen as shape-directing agent, which could naturally attach on the surface of negatively charged GO sheets and then modify the electronegativity of GO substrate. Once biomass glucose with negative charges was added, it could be also driven by electrostatic force to be close to the modified GO-NH_2 sheets. This idea was confirmed by the Zeta potential measurements. The Zeta potential of the original GO was -51.0 mV, while after the adding of EDA, the value changed to -13.4 mV, which demonstrated the modification of -NH_2 terminal of EDA on the surface charge property of GO. When glucose was further added, the Zeta potential decreased to -39.7 mV, which suggested the attachment of glucose molecules on EDA-modified GO. So EDA was expected to be acted as a binder to connect negatively charged glucose and GO. The following hydrothermal treatment resulted in the carbonization of glucose on the surface of GO, so that hydrothermal carbons (HTCs) uniformly coated on both sides of reduced GO sheets to form a sandwich-type structure. Finally, after KOH activation at high temperature, porous carbon composites were formed, which would combine the merits of the good electrical conductivity of graphene and the rich porosity of hydrothermal carbon together.

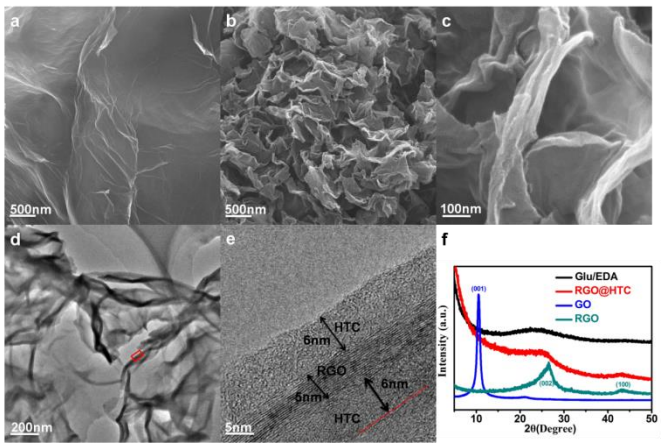

Fig. 2 SEM images of (a) rGO and (b, c) RGO@HTC; (d)TEM and (e) HRTEM images of RGO@HTC (The section marked by the red block is the location of HRTEM); and (f) XRD patterns of RGO@HTC, Glu/EDA, rGO and GO.

As we know, carbonaceous materials prepared by hydrothermal methods are generally sensitive to experimental conditions, such as carbon precursor, additive, reactant ratio and activation temperature. So according to Fig. 1, a series of experiments were designed and processed to search the optimized conditions. Up to now, the expected RGO@HTC composites could be successfully prepared after hydrothermal treatment at 180 ºC for 10 h with a moderate Glucose/GO weight ratio of 100:1 and a addition of 1 ml EDA, followed by KOH activation at 600 ºC for 2 h with a Carbon/KOH weight ratio of 2:1. The morphology and structure of the optimal RGO@HTC materials are showed in Fig. 2. The SEM image (Fig. 2b) obviously indicated that the RGO@HTC composites presented a plate-like morphology and these wrinkled plates formed a lot of uniformly distributed macropores, completely different from the pure GO morphology (Fig. 2a). The resulting macroporosity would serve in electrochemical applications as ion-buffering reservoirs to facilitate charge transport, especially at high current density and high mass loading.[39,40] The magnified SEM image (Fig. 2c) clearly revealed that these plates were about several hundred nm in edge length and 20 nm in thickness. Moreover, the presence of wrinkled plates could prevent these neighboring plates from stacking with each other, thus to the largest extent, maintaining the effective surface area. To certify the necessary of reactants, two control samples were prepared under the same conditions except for the absence of

GO or EDA, respectively denoted as Glu/EDA and Glu/GO. As shown in Fig. S1, without the support of GO or EDA, the hydrothermal treatment of glucose only produced carbonaceous spheres like these previous reports.[39,41] Especially for Glu/GO, HTCs spheres and GO sheets grew individually, which might be explained that the negative charges of HTCs inherited from these functional groups of glucose caused electrostatic repulsion to force nucleation and growth of hydrothermal carbon far away from negatively charged GO. It significantly confirmed the importance of EDA with two $-NH_2$ terminals to the unique morphology of RGO@HTC.

To obtain further insight into the RGO@HTC plates, TEM and HRTEM measurements were used. In the TEM image (Fig. 2d), some similar wrinkled plates were observed in agreement with the SEM results. And the separated GO or HTCs phases could not be found at all, suggesting two kinds of carbon materials were perfectly combined together. The HRTEM image (Fig. 2e) confirmed a sandwich-type structure of RGO@HTC composites. The crystallized GO and amorphous HTCs could be obviously distinguished on the cross section of an individual RGO@HTC plate. The thickness of the central GO with clear lattice planes was about 5 nm, implying that the overlapped graphene layers were just a few. The both sides of GO were completely coated by some amorphous carbon layers coming from hydrothermal carbonization of glucose. Each HTCs layer was about 6 nm in thickness. The sandwich-type carbon composites could inherit a good electrical conductivity from GO and ensure a sufficient exfoliation of GO sheets due to the covering of amorphous HTCs. The presence of amorphous carbon layers was further confirmed by the Raman spectrum of RGO@HTC (Fig. S2). The intensity ratio (I_D/I_G) of the D band and G band was high, and the strong D band demonstrated that the RGO@HTC had a low graphitization degree and contained a plenty of disordered sections and defects, which was consistent with the typical amorphous porous carbons.[42] By comparison with a low I_D/I_G of Glu/EDA, the introduction of GO into the system could influence the hydrothermal process and graphitization degree of glucose molecules. Moreover, the crystal structure of the RGO@HTC was studied by XRD (Fig. 2f). Different from that of the GO reactant, the diffraction peak at 10.6° belonging to the (001) crystal facet of GO disappeared but two broad peaks at 26.4° and 43.0° were observed, which could be attributed to the (002) and (100) crystal facets of rGO. The result revealed that the most oxygen functional groups of GO had been removed in the structure of RGO@HTC, which would lead to a further increase in electrical conductivity. And the peak at 26.4° was relatively broad and displayed the similar shape to that of Glu/EDA, which was the characteristic of the outer amorphous HTCs layers. In addition, a rapid increase at the low angle was also observed, which was probably related to the presence of much more pores.[17] To estimate the graphene percent in the carbon composites, a control experiment was carried out and shown in Table S1. After the same hydrothermal treatment and KOH activation, 0.200 g of pure GO decreased to 0.025 g and the mass loss percent of GO was almost 87.5%. But the remaining mass was 0.140 g for the RGO@HTC reaction system with an original mass of about 4.040 g (4 g glucose, 1 ml EDA and 0.040 g GO). If assuming the reduction degrees of GO in two systems were similar, 0.040 g GO should decrease to 0.005 g and only account for about 3.6 wt% of RGO@HTC. So the rest part of RGO@HTC, about 96.4% should be derived from the glucose carbonization. The calculation result verified again that the HTCs successfully coated the rGO. And the significantly increased mass of the final composites could effectively offset the shortcoming of low productivity of rGO, which would potentially pave the pathway for practical supercapacitor applications.

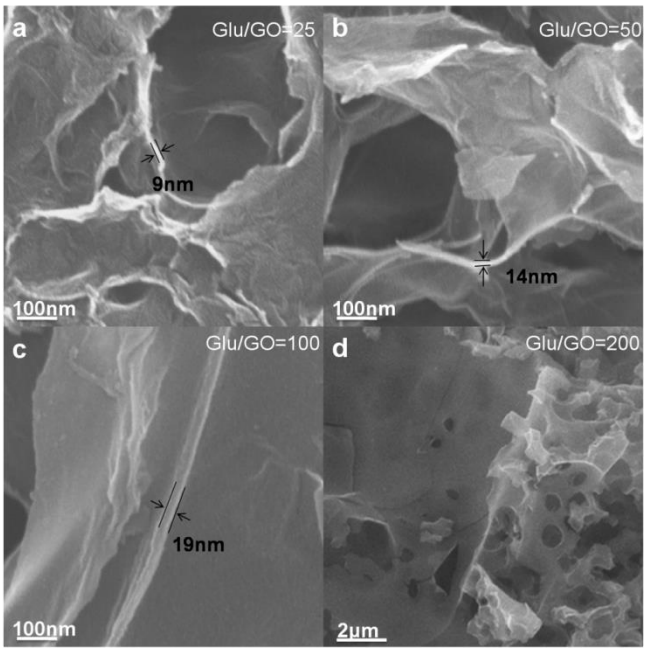

Fig. 3 SEM images of the carbonaceous composites prepared at different Glucose/GO weight ratios: (a) 25:1, (b) 50:1, (c) 100:1, and (d) 200:1.

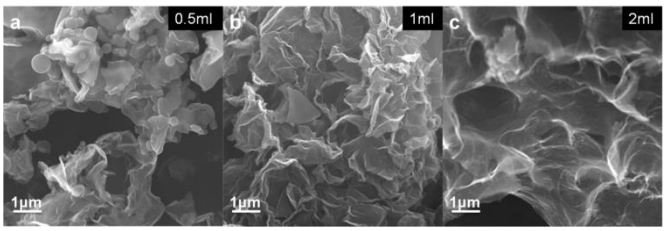

Fig. 4 SEM images of the carbonaceous composites prepared at different EDA amounts: (a) 0.5 mL, (b) 1 mL, and (c) 2 mL.

The effects of various experimental conditions on morphology and structure of the RGO@HTC composites were systematically investigated. Firstly, the reactant weight ratio of glucose to GO varied from 25:1, 50:1, 100:1, up to 200:1 with a fixed EDA amount of 1 mL, and other reaction conditions were same (hydrothermal treatment at 180 °C for 10 h, followed by KOH activation with a Carbon/KOH weight ratio of 1:1 at 600 °C for 2 h). SEM images of the resulting samples are

shown in Fig. 3. When the Glucose/GO weight ratios were less than 100:1, these samples performed wrinkled plate-like morphologies, similar to the optimal sample in Fig. 2. The primary difference of three samples was sheet thickness, which increased from 9, 14 up to 19 nm with the ratio change from 25:1 to 100:1. The result indicated that the HTCs layers successfully coated the surface of graphene and thickened with the glucose amount increasing. However, when the Glucose/GO ratio reached to 200:1, the morphology completely changed (Fig. 3d). Many bulk materials with large pores were observed, which might be explained that the carbonization of the excess glucose molecules preferred to take place in the solution rather than on the surface of GO. Obviously, the bulk materials had a small specific surface area and low electrical conductivity due to the lack of GO by comparison with the others. So a moderate Glucose/GO ratio was important to the formation of the sandwich-type RGO@HTC materials and herein 100:1 was chosen as the best one.

To study the importance of EDA during the formation process of the RGO@HTC, the amount of EDA was tuned from 0, 0.5, 1 to 2 mL and other experimental conditions remained the same (hydrothermal treatment with a Glucose/GO weight ratio of 100:1 at 180 °C for 10 h, followed by KOH activation with a Carbon/KOH weight ratio of 1:1 at 600 °C for 2 h). As mentioned in Fig. S1b, the reaction system without EDA only produced individual carbon spheres and graphene sheets. When the EDA amount was 0.5 mL, some wrinkled plates began to appear besides some carbon microspheres (Fig. 4a). Once the EDA amount increased to 1 mL and more, the microspheres completely disappeared and the expected plates occupied all the view as shown in Fig. 4b. Therefore, we concluded that EDA was the most important factor for the formation of HTCs coating rGO. It acted as a "binder" to connect negatively charged GO and glucose depending on its two $-NH_2$ terminals. When the EDA amount was insufficient, a part of glucose molecules could not be glued to the surface of GO and so they entered into the solution to form spherical carbons after hydrothermal treatment. Conversely, when the EDA amount was sufficient (more than 1 mL), all the added glucose molecules could be carbonized on GO to develop the sandwich-type carbon composites. Moreover, the plates became thin and more pores appeared with the addition of 2 mL EDA (Fig. 4c), which might be related to the etching of more NH_3/NO_x bubbles. So a moderate EDA amount was quite important to the formation of the sandwich-type RGO@HTC and herein 1 mL was chosen as the best one.

Recent studies showed that various carbons had been etched by KOH activation to introduce additional micropores and small mesopores into the frameworks, thus greatly improving the specific surface areas as well as the capacitive performances.[43,44] The KOH effect was investigated in a series of the RGO@HTC composites activated at different Carbon/KOH weight ratios from 4:1, 3:1, 2:1, 1:1, up to 1:2, and other conditions remained like the optimal ones. The morphology evolution was measured by SEM, and the images of the typical composites with Carbon/KOH ratios of 4:1 and 1:2 are showed in Fig. 5a and 5b, respectively. It was observed that KOH activation did not change the unique plate-like morphology of RGO@HTC but the sheet thickness varied with KOH amount. When the Carbon/KOH ratio decreased to 1:2, the carbonaceous composite became relatively thin and had insufficient mechanical strength even leading to a structure collapse because of KOH serious etching. Moreover, the N_2 sorption measurements were conducted to further investigate the pore structures of the prepared samples as displayed in Fig. 5c and 5d. Obviously, these N_2 sorption isotherms showed a representative type-IV isotherm, which indicated the mesoporous characteristic of the solid materials. With KOH amount increasing, the isotherms presented a certain volume adsorption when the P/P_0 decreased to 0.4 and below, suggesting the microporous channel distribution. It was also confirmed by the specific surface area (SSA) evolution in Table S2: the SSAs increased from 1240 to 2745 $m^2\ g^{-1}$ with the Carbon/KOH ratio decreasing, which was associated with rich porosity. Though every sample had a narrow pore size distribution in the range of 2-3 nm as shown in Fig. 5d, the sample with a moderate Carbon/KOH ratio of 2:1 displayed the sharpest and strongest peak, and it had the highest mesopore volume of 0.405 $cm^3\ g^{-1}$ with a large SSA of 1749 $m^2\ g^{-1}$. Recent years, to optimize the performances of these capacitors, numerous efforts had been devoted to 3D carbon materials with multifold pore structures.[40,45] Therefore, the RGO@HTC composites possessed a hierarchical porous network in terms of micro-, meso- and macro- pores as well as a much richer porosity, which would show promise as a kind of good electrode materials for supercapacitors.

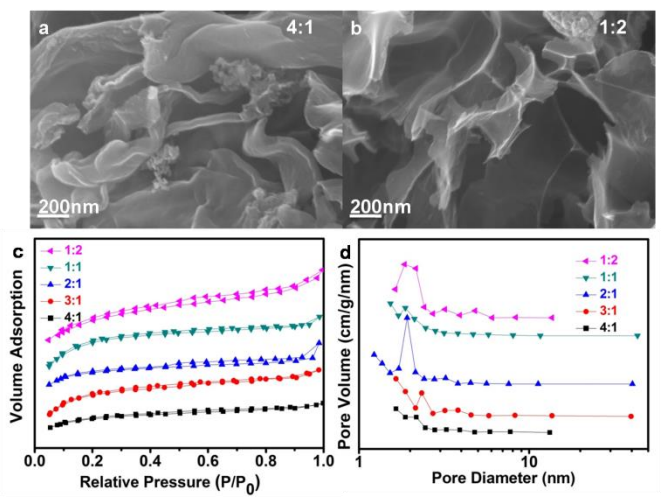

Fig. 5 SEM images of the carbonaceous composites activated at different Carbon/KOH weight ratios: (a) 4:1, (b) 1:2; (c) their N_2 adsorption/desorption isotherms and (d) pore size distributions.

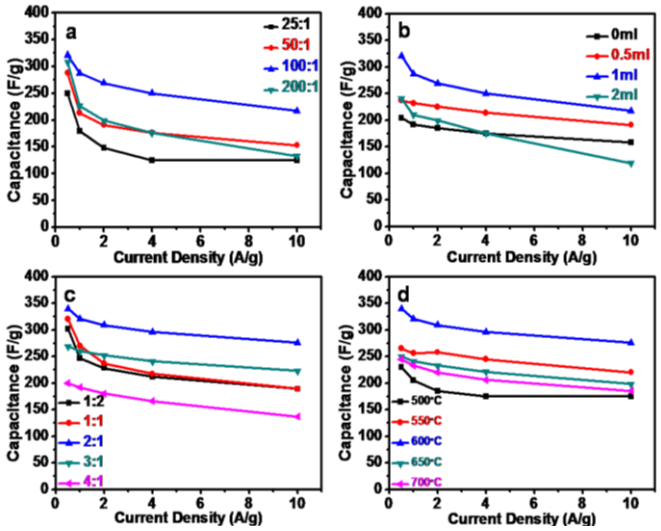

Fig. 6 The specific capacitance evolutions of the carbonaceous composites prepared at different conditions vs. the charge/discharge current densities in 6 mol L^{-1} KOH: (a) different Glucose/GO weight ratios of 25:1, 50:1, 100:1, 200:1 (Carbon/KOH weight ratio of 1:1), (b) different EDA amount of 0 , 0.5, 1, 2 mL (Carbon/KOH weight ratio of 1:1), (c) different Carbon/KOH weight ratios of 4:1, 3:1, 2:1, 1:1, 1:2, and (d) different activation temperatures of 500, 550, 600, 650, 700°C.

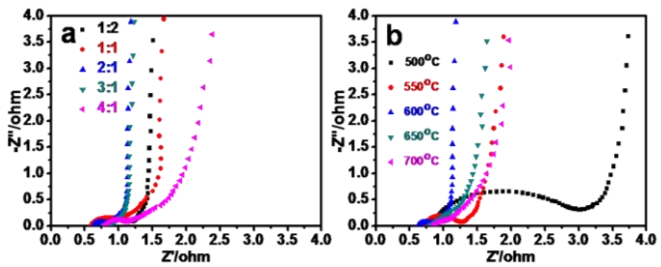

Fig. 7 EIS plots of the carbonaceous composites activated at different conditions: (a) different Carbon/KOH weight ratios of 4:1, 3:1, 2:1, 1:1, 1:2, and (b) different activation temperatures of 500, 550, 600, 650, 700°C.

To further investigate the effect of various experimental conditions on electrochemical performances of the RGO@HTC composites, the specific capacitances calculated from the results of charge/discharge profiles versus current densities are depicted in Fig. 6. As shown in Fig. 6a, the specific capacitances increased with an increase of Glucose/GO weight ratio from 25:1 to 100:1 and then decreased when the ratio reached up to 200:1 at any chosen current densities from 0.5 A g^{-1} to 10 A g^{-1}. The RGO@HTC with a Glucose/GO ratio of 100:1 possessed the maximum capacitances. And it retained high capacitance retention of 68% at 10 A g^{-1} by comparison to others. This could be well explained by the morphological and structural evolution of the composites prepared at different Glucose/GO ratios in Fig. 3. With the ratio increasing, the amount of porous HTCs covering on the surface of rGO sheets enhanced, which increasingly influenced the surface properties and thus restrained restacking and aggregation of rGO sheets. It probably led to the formation of the wrinkled plate-like morphology with large effective surface area and hierarchical porous structure, which was conducive to a faster ion and electron migration in the charge/discharge process.[37,46] Moreover, the sufficient amount of the reductive glucose was relative to the high graphitization degree of rGO sheets after hydrothermal treatment, which possibly benefited electric conductivity of the final products. So, the RGO@HTC with a Glucose/GO ratio of 100:1 delivered the best specific capacitance and rate performance. When the ratio reached to 200:1, the carbon composites lost the plate-like morphology and turned to the bulk, which caused the decrease of SSA and porosity, and thus hindered the electrochemical performance. Fig. 6b illustrated that the specific capacitances gradually increased with the increase of EDA amount from 0 to 1 mL. Combined with Fig. 4, it was found that the specific capacitances were well corresponding to the morphology change of the composites: the RGO@HTC prepared at 1 mL EDA showed the complete disappearance of carbonaceous spheres and the presence of sandwich-type plates. So the as-prepared plates were desirable for fabricating the conductive and porous electrodes for supercapacitators. Instead, the capacitance dropped when the EDA amount continued increasing to 2 mL, which was probably relevant to the carbonaceous plate thinning. As seen in Fig. 6c, the ratio of carbon to activating agent (KOH) had a significant impact on electrochemical performances of the prepared carbonaceous composites. The specific capacitance firstly enhanced with the Carbon/KOH ratio increasing, consistent with the increase of SSA and pore volume. The RGO@HTC composites with a Carbon/KOH ratio of 2:1 displayed the best performance. But then, the capacitance faded once the Carbon/KOH ratio continued increasing, which was opposite with the change of SSA. According to Fig. 5b, it might be resulted from the fact that excessive KOH etching led to the structure collapse and then influenced the electrical conductivity. In addition, electrochemical impedance spectroscopy was used to detect their electrical conductivities. The results are shown in Fig. 7a. Clearly, the semicircle diameter of Nyquist plot of the RGO@HTC composites with a Carbon/KOH ratio of 2:1 was the smallest in the high-frequency region, indicating that the materials offered fast charge transportation and possessed low contact resistance.[47] Though the carbonaceous composites with a Carbon/KOH ratio of 1:2 possessed the largest SSA, the specific capacitance was not the highest one, which was mainly attributed to a poor electrical conductivity. The result confirmed the electrical conductivity as one of the important explanation for the high capacitance. The effect of activation temperature on supercapacitor performances is illustrated in Fig. 6d. The specific capacitance of the sample activated at 600 °C was always the highest at any chosen current density. It was observed in Fig. 7b that the Nyquist plot of the sample activated at 600 °C displayed the smallest semicircle in the high-frequency region. Lower activation temperatures could not yield abundant micropores from the C-KOH reaction, leading to lower porosity. And incomplete thermal treatments often

cause poor graphitization degree. However, too high activation temperatures could significantly increase the C-KOH reaction rate and then result in the burn-off of some carbon structures and the widening of micropores to meso- and macropores.[48,49] Because the capacitance decreases with the increase of pore size, depletion of micropores would lead to the decrease of useful pores for supercapacitor, especially when specific surface area and total pore volume was compromised, too. Therefore, the moderate KOH activation temperature was necessary for the preparation of carbon materials with good electrochemical performance. Herein we chose 600 °C as the optimal activation temperature.

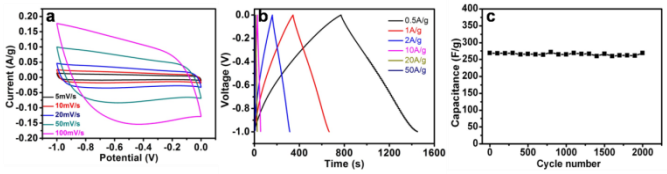

Fig. 8 Electrochemical performances of RGO@HTC in 6 mol L^{-1} KOH: (a) CV curves at different scanning rates, (b) GCD curves at different current densities, and (c) cycling stability at a current density of 10 A g^{-1} in 1 mol L^{-1} KOH.

Briefly, a series of control experiments helped us to find the optimized conditions at the moment. To investigate the excellent performance of the optimal RGO@HTC composites as supercapacitor electrodes, various electrochemical measurements were performed including cyclic voltammetry (CV), galvanostatic charge-discharge (GCD) and electrochemical impedance spectroscopy (EIS) in 6 mol L^{-1} KOH aqueous solution. Fig. 8a depicts the CV curves of the RGO@HTC at different scanning rates from 5 to 100 mV s^{-1}. The curves maintained quasi-rectangular shaped voltammetry characteristics at low scanning rates (< 50 mV s^{-1}), indicating the electrical double-layer capacitive behavior of the carbon composites. However, when the scanning rate increased to 50 mV s^{-1} and above, the shapes exhibited increased distortion from the typical rectangular shape, which mainly resulted from the inherent inner resistance as well as the pseudocapacitance contribution related to the heteroatoms (doped N) in the electrode materials. Moreover, with the scanning rate increasing, the current density increased clearly, indicating good rate ability. As presented in Fig. 8b, the slight deviations from the linear characteristics were observed in the GCD tests, suggesting the presence of faradic reactions derived from doped N atoms during the charge/discharge process. Estimated from them, the specific capacities of the RGO@HTC achieved 340 F g^{-1} at a current density of 0.5 A g^{-1} and 321 F g^{-1} at 1 A g^{-1}, higher than most of the reported GO-related carbon materials as listed in Table 1.[17,18,30,46,50-54] In addition, the capacitance still remained 276 F g^{-1} at a high current density of 10 A g^{-1} and 203 F g^{-1} even at 50 A g^{-1}, indicating a good rate capability. The comparative cycling stability of the RGO@HTC at a constant current density of 10 A g^{-1} was measured and shown in Fig. 8c. It displayed a remarkably stable capacitance, without any degradation even after 2000 cycles of charge/discharge process. By comparison with other electrode materials partly containing pseudocapacitance, the excellent cycling stability suggested the faradic reactions based on the doped N being fully reversible, which might be ascribed to the N-containing functional groups strongly bonding with the carbon and remaining stable during cycling. In conclusion, the sandwich-type RGO@HTC composites exhibited a remarkable specific capacitance, rate capability and cycling stability as we expected.

Table 1 Specific capacitance data in our work and some references.

Sample	Electrolyte	Current density or scan rate	Capacitance (F g^{-1})	Reference
a-MEGO	$(BMIMBF_4)$/AN	0.8 A g^{-1}	150	17
r[GO-CNT]	1 M TEABF4	1 A g^{-1}	109.1	51
cMR-rGO	1 M $LiPF_6$	1 A g^{-1}	203	52
RGO	6 M KOH	1 A g^{-1}	190	18
CNT/graphene	6 M KOH	10 mV s^{-1}	385	53
GNS/MnO_2	1 M Na_2SO_4	0.67 A g^{-1}	227	54
Graphene	5 M KOH	0.1 A g^{-1}	155	46
MLG/PC	1 M Na_2SO_4	20 A g^{-1}	173	50
Graphene	0.5 M NaCl	0.6 A g^{-1}	230	30
RGO@HTC	6 M KOH	1 A g^{-1}	321	Our work
	6 M KOH	50 A g^{-1}	203	Our work

To reveal the "intrinsic properties" that dominating the excellent electrochemical performances of the RGO@HTC, we further studied and discussed the important roles of structure and composition. Firstly, as mentioned above, it was closely relevant to the presence of a hierarchical pore network of carbon materials, which provided more interconnected channels to facilitate ions transportation and reduce diffusion distance. Combining the merits of porous HTCs and large-area rGO substrate effectively, the unique sandwich-type RGO@HTC plates displayed an improved specific surface area and pore volume, which guaranteed more ions could participate in the electrical double-layer formation. In addition, the covering of HTCs on the surface of rGO prevented rGO sheets from agglomerating and stacking, then ensuring more exposed surfaces.

Secondly, it was relevant to the presence of an amount of doped N atoms. During the preparation process of the RGO@HTC, EDA with two $–NH_2$ terminals acted not only as a binder to help the hydrothermal carbonization of glucose molecules on the surface of GO sheets, but also as a nitrogen source to realize in-situ doping of N atoms into the framework. The contents of the element C, N on the surface of RGO@HTC and Glu/EDA were respectively evaluated using X-ray photoelectron spectroscopy (XPS). Their XPS spectra are illustrated in Fig. 9 and the detailed information are summarized in Table S3 and S4. In Fig. 9b, the significant N1s peak of the RGO@HTC was recorded, which confirmed the

successful N-doping in the composites using our experimental method. The N content on the surface calculated from the XPS result is 7.34 at%, higher than that of the GO-free Glu/EDA (4.26 at%, Fig. 9a). It demonstrated that the introduction of GO not only changed the morphology of the HTCs, but also assisted the N-doping. The N1s spectra of two samples could be fitted with three different signals of pyridine N, pyrrolic N and quaternary-N at about 399.0, 399.9 and 400.8 eV, respectively.[55] By comparison with Glu/EDA, the content of nitrogen in pyridine form enhanced while other forms reduced for RGO@HTC. It is well known that nitrogen doping is a simple but effective process for carbon materials to improve their performances or extend their function.[47,55,56] Particularly in supercapacitors, N-doping endows carbon materials with pseudocapacitance based on its faradic reactions. So we believed that the N-doping enhancement in the RGO@HTC composition was one of fundamental factors being responsible for their excellent electrochemical performances.

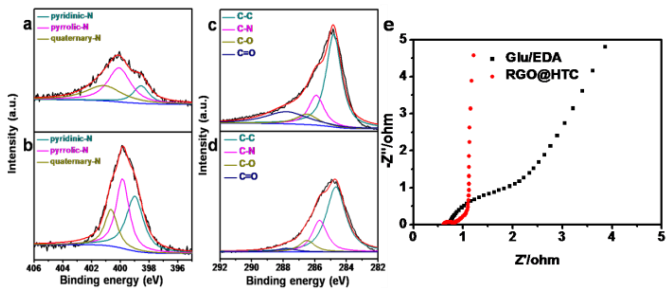

Fig. 9 (a) N1s and (c) C1s XPS spectra of Glu/EDA, (b) N1s and (d) C1s XPS spectra of RGO@HTC, and (e) EIS plots of two samples in 6 mol L^{-1} KOH.

Thirdly, it was relevant to the presence of super electrical conductivity derived from rGO, which was confirmed by XPS and EIS measurements. The C1s XPS spectrum of the RGO@HTC in Fig. 9d could be split to four peaks, respectively attributed to sp^2 carbon (284.8 eV), carbon in C-N (285.9 eV), carbon in C-O (286.5 eV), and carbon in carbonyl (287.8 eV),[51] which was similar to that of the control sample Glu/EDA in Fig. 9c. The locations and atomic percents of carbon functionalities are displayed in Table S4, and the relative percents of the corresponding carbon functionalities were significantly different for two samples. For the GO-containing sample, the carbon contents in C-O and C=O decreased, especially the carbonyl carbon decreasing from 15.8 at% to 2.8 at%, which suggested a better electrical conductivity. Moreover, the obvious increase of carbon in C-N was consistent with the N-doping enhancement. The super electrical conductivity was further confirmed by EIS results. As shown in Fig. 9e, the semicircle diameter of Nyquist plot of the RGO@HTC in the high-frequency region was smaller than that of the Glu/EDA, and both the series resistance (Rs, 0.6 Ω) and the charge-transfer resistance (Rct, 0.2 Ω) of the RGO@HTC were relatively low. Moreover, the nearly vertical line of Nyquist plot of the RGO@HTC in the low-frequency range proved much better electrochemical capacitive properties of the materials.[57] So the introduction of GO assisted the improvement of the electrical conductivity of the RGO@HTC. From what had been discussed above, we believed that by virtue of the combination of conductive graphene and porous HTCs, the RGO@HTC composites showed a large surface area, appropriate hierarchical pore structure, high N content, and excellent electrical conductivity, so that resulting in good supercapacitor performances.

4 Conclusions

Graphene based N-doped RGO@HTC composites were prepared by a facile and economical route. The resulting carbon materials presented sandwich-type wrinkled plates, in which porous hydrothermal carbon uniformly covered on the surface of rGO sheets. The utilization of EDA with two amino terminals was a key factor to connect negatively charged glucose molecules to GO together. The materials possessed supercapacitor performances much superior to most of other GO based carbon electrodes. The excellent structural characteristics of the RGO@HTC materials might be ascribed to the following aspects: (a) the high specific surface area and appropriate hierarchical pore structure easily accessible to electrolyte were helpful for large amounts of charge storage; (b) the high nitrogen content on the carbon surface brought pseudocapacitance due to the faradic reactions and improved the wettability which enhanced the utilization efficiency of the surface area; (c) the introduction of rGO accelerated the charge transportation to enhance the electrical conductivity of the carbon composites. The optimal RGO@HTC composites under the current conditions exhibited high specific capacitance (340 F g^{-1} at 0.1 A g^{-1}), excellent rate capability (203 F g^{-1} at 50 A g^{-1}) and good cycling stability (nearly no capacity decay over 2000 cycles) in 6 mol L^{-1} KOH aqueous electrolyte, making them promising electrode materials for supercapacitors.

Acknowledgements

This work was financially supported by the National Natural Science Foundation of China, the 973 Program (2011CBA00503, 2011CB932403), Changjiang Scholars and Innovative Research Team in University (IRT1205), the Fundamental Research Funds for the Central Universities (YS1406).

Notes and references

Huaxing Luo, Lumeng Chao, Xiaochao Wu, Dr. Xiaodong Lei, Dr. Zheng Chang, Prof. Xiaoming Sun
State Key Laboratory of Chemical Resource Engineering, Beijing University of Chemical Technology, Beijing 100029, China.
Dr. Zhenyu Liu
Maoming Branch R&D Institute, SINOPEC, Maoming 525011, China
Email: changzheng@mail.buct.edu.cn; sunxm@mail.buct.edu.cn
Fax: +86-10-64425385; Tel: +86-10-64448751
Electronic Supplementary Information (ESI) available: [supplementary SEM iamges , Raman spectra, XPS spectra and Table.]. See DOI: 10.1039/b000000x/

1 D. S. Su and G. Centi, *J. Energ. Chem.*, 2013, **22**, 151-173.
2. G. Wang, L. Zhang and J. Zhang, *Chem. Soc. Rev.*, 2012, **41**, 797-828.
3. M. Winter and R. J. Brodd, Chem. Rev., 2004, 104, 4245-4270.
4. H.-J. Choi, S.-M. Jung, J.-M. Seo, D. W. Chang, L. Dai and J.-B. Baek, *Nano Energy*, 2012, **1**, 534-551.
5. Y. Zhao, J. Liu, Y. Hu, H. Cheng, C. Hu, C. Jiang, L. Jiang, A. Cao and L. Qu, *Adv. Mater.*, 2013, **25**, 591-595.
6. M. Vangari, T. Pryor and L. Jiang, *J. Energy Eng.*, 2013, **139**, 72-79.
7. W. Huang, H. Zhang, Y. Huang, W. Wang and S. Wei, *Carbon*, 2011, **49**, 838-843.
8. Q. Li, R. Jiang, Y. Dou, Z. Wu, T. Huang, D. Feng, J. Yang, A. Yu and D. Zhao, *Carbon*, 2011, **49**, 1248-1257.
9. M. Kaempgen, C. K. Chan, J. Ma, Y. Cui and G. Gruner, *Nano Lett.*, 2009, **9**, 1872-1876.
10. S. Nardecchia, D. Carriazo, M. L. Ferrer, M. C. Gutierrez and F. del Monte, *Chem. Soc. Rev.*, 2013, **42**, 794-830.
11. G. Xu, C. Zheng, Q. Zhang, J. Huang, M. Zhao, J. Nie, X. Wang and F. Wei, *Nano Res.*, 2011, **4**, 870-881.
12. Y. Lv, L. Gan, M. Liu, W. Xiong, Z. Xu, D. Zhu and D. S. Wright, *J. Power Sources*, 2012, **209**, 152-157.
13. X. Ma, L. Gan, M. Liu, P. K. Tripathi, Y. Zhao, Z. Xu, D. Zhu and L. Chen, *J. Mater. Chem. A*, 2014, **2**, 8407-8415.
14. M. Liu, L. Gan, W. Xiong, Z. Xu, D. Zhu and L. Chen, *J. Mater. Chem. A*, 2014, **2**, 2555-2562.
15. J. Qian, M. Liu, L. Gan, P. K. Tripathi, D. Zhu, Z. Xu, Z. Hao, L. Chen and D. S. Wright, *Chem Commun (Camb)*, 2013, **49**, 3043-3045.
16. Y. Zhao, M. Liu, L. Gan, X. Ma, D. Zhu, Z. Xu and L. Chen, *Energ. Fuel.*, 2014, **28**, 1561-1568.
17. Y. Zhu, S. Murali, M. D. Stoller, K. J. Ganesh, W. Cai, P. J. Ferreira, A. Pirkle, R. M. Wallace, K. A. Cychosz, M. Thommes, D. Su, E. A. Stach and R. S. Ruoff, *Science*, 2011, **332**, 1537-1541.
18. Z. Lei, L. Lu and X. S. Zhao, *Energy Environ. Sci.*, 2012, **5**, 6391-6399.
19. C. Xu, B. Xu, Y. Gu, Z. Xiong, J. Sun and X. S. Zhao, *Energy Environ. Sci.*, 2013, **6**, 1388-1414.
20. H. Wang, Y. Liang, T. Mirfakhrai, Z. Chen, H. Casalongue and H. Dai, *Nano Res.*, 2011, **4**, 729-736.
21. A. Olejniczak, M. Lezanska, J. Wloch, A. Kucinska and J. P. Lukaszewicz, *J. Mater. Chem. A*, 2013, **1**, 8961.
22. C. Falco, M. Sevilla, R. J. White, R. Rothe and M. M. Titirici, *ChemSusChem*, 2012, **5**, 1834-1840.
23. M.-M. Titirici, R. J. White, C. Falco and M. Sevilla, *Energy Environ. Sci.*, 2012, **5**, 6796-6822.
24. Z. Wen, X. Wang, S. Mao, Z. Bo, H. Kim, S. Cui, G. Lu, X. Feng and J. Chen, *Adv. Mater.*, 2012, **24**, 5610-5616.
25. Z. Liu, J. T. Robinson, X. Sun and H. Dai, *J. Am. Chem. Soc.*, 2008, **130**, 10876-10877.
26. Z. Tang, S. Shen, J. Zhuang and X. Wang, *Angew. Chem., Int. Ed.*, 2010, **122**, 4707-4711.
27. C. Liu, Z. Yu, D. Neff, A. Zhamu and B. Z. Jang, *Nano Lett.*, 2010, **10**, 4863-4868.
28. Y. Zhu, M. D. Stoller, W. Cai, A. Velamakanni, R. D. Piner, D. Chen and R. S. Ruoff, *Acs Nano*, 2010, **4**, 1227-1233.
29. J. Xia, F. Chen, J. Li and N. Tao, *Nat. Nanotechnol.*, 2009, **4**, 505-509.
30. H. Wang, D. Zhang, T. Yan, X. Wen, L. Shi and J. Zhang, *J. Mater. Chem.*, 2012, **22**, 23745-23748.
31. K. S. Novoselov, V. I. Fal'ko, L. Colombo, P. R. Gellert, M. G. Schwab and K. Kim, *Nature*, 2012, **490**, 192-200.
32. L. Chen, Y. Hernandez, X. Feng and K. Mullen, *Angew. Chem., Int. Ed.*, 2012, **51**, 7640-7654.
33. D. K. James and J. M. Tour, *Accounts Chem. Res.*, 2012, **46**, 2307-2318.
34. A. Bianco, *Angew. Chem., Int. Ed.*, 2013, **52**, 4986-4997.
35. Y. Zhu, S. Murali, W. Cai, X. Li, J. W. Suk, J. R. Potts and R. S. Ruoff, *Adv. Mater.*, 2010, **22**, 3906-3924.
36. D. Krishnan, K. Raidongia, J. Shao and J. Huang, *ACS Nano*, 2013, **8**, 449-457.
37. X. Fan, C. Yu, J. Yang, Z. Ling and J. Qiu, *Carbon*, 2014, **70**, 130-141.
38. D. Luo, G. Zhang, J. Liu and X. Sun, *J. Phys. Chem. C*, 2011, **115**, 11327-11335.
39. M.-M. Titirici, M. Antonietti and N. Baccile, *Green Chem.*, 2008, **10**, 1204-1212.
40. B. Hu, K. Wang, L. Wu, S. H. Yu, M. Antonietti and M. M. Titirici, *Adv. Mater.*, 2010, **22**, 813-828.
41. Z. Gao, W. Yang, J. Wang, H. Yan, Y. Yao, J. Ma, B. Wang, M. Zhang and L. Liu, *Electrochim. Acta*, 2013, **91**, 185-194.
42. G. Eda and M. Chhowalla, *Adv. Mater.*, 2010, **22**, 2392-2415.
43. J. Wang and S. Kaskel, *J. Mater. Chem.*, 2012, **22**, 23710-23725.
44. M. Choi and R. Ryoo, *J. Mater. Chem.*, 2007, **17**, 4204-4209.
45. L. Qie, W. Chen, H. Xu, X. Xiong, Y. Jiang, F. Zou, X. Hu, Y. Xin, Z. Zhang and Y. Huang, *Energ. Environ. Sci.*, 2013, **6**, 2497-2504.
46. L. Jiayan, J. Hee Dong and H. Jiaxing, *Acs Nano*, 2013, **7**, 1464-1471.
47. X. Li, X. Zang, Z. Li, X. Li, P. Li, P. Sun, X. Lee, R. Zhang, Z. Huang, K. Wang, D. Wu, F. Kang and H. Zhu, *Adv. Funct. Mater.*, 2013, **23**, 4862-4869.
48. J. Wang and S. Kaskel, *J. Mater. Chem.*, 2012, **22**, 23710-23725.
49. A. C. Lua and Ting Yang, *J. Colloid Interf. Sci.*, 2004, **274**, 594-601.
50. M. Zhong, E. K. Kim, J. P. McGann, S.-E. Chun, J. F. Whitacre, M. Jaroniec, K. Matyjaszewski and T. Kowalewski, *J. Am. Chem. Soc.*, 2012, **134**, 14846-14857.
51. N. Jung, S. Kwon, D. Lee, D. M. Yoon, Y. M. Park, A. Benayad, J. Y. Choi and J. S. Park, *Adv. Mater.*, 2013, **25**, 6854-6858.
52. J. H. Lee, N. Park, B. G. Kim, D. S. Jung, K. Im, J. Hur and J. W. Choi, *Acs Nano*, 2013, **7**, 9366-9374.
53. Z. Fan, J. Yan, L. Zhi, Q. Zhang, T. Wei, J. Feng, M. Zhang, W. Qian and F. Wei, *Adv. Mater.*, 2010, **22**, 3723-3728.
54. W. Yang, Z. Gao, J. Wang, B. Wang, Q. Liu, Z. Li, T. Mann, P. Yang, M. Zhang and L. Liu, *Electrochim. Acta*, 2012, **69**, 112-119.

55. D. Hulicova-Jurcakova, M. Kodama, S. Shiraishi, H. Hatori, Z. H. Zhu and G. Q. Lu, *Adv. Funct. Mater.*, 2009, **19**, 1800-1809.
56. K. N. Wood, R. O'Hayre and S. Pylypenko, *Energ. Environ. Sci.*, 2014, **7**, 1212-1249.
57. X. Wen, D. Zhang, T. Yan, J. Zhang and L. Shi, *J. Mater. Chem. A*, 2013, **1**, 12334-12344.

